



# Improvements in Modeling 90° Bleed Holes for Supersonic Inlets

*John W. Slater*  
*Glenn Research Center, Cleveland, Ohio*

## NASA STI Program . . . in Profile

Since its founding, NASA has been dedicated to the advancement of aeronautics and space science. The NASA Scientific and Technical Information (STI) program plays a key part in helping NASA maintain this important role.

The NASA STI Program operates under the auspices of the Agency Chief Information Officer. It collects, organizes, provides for archiving, and disseminates NASA's STI. The NASA STI program provides access to the NASA Aeronautics and Space Database and its public interface, the NASA Technical Reports Server, thus providing one of the largest collections of aeronautical and space science STI in the world. Results are published in both non-NASA channels and by NASA in the NASA STI Report Series, which includes the following report types:

- **TECHNICAL PUBLICATION.** Reports of completed research or a major significant phase of research that present the results of NASA programs and include extensive data or theoretical analysis. Includes compilations of significant scientific and technical data and information deemed to be of continuing reference value. NASA counterpart of peer-reviewed formal professional papers but has less stringent limitations on manuscript length and extent of graphic presentations.
- **TECHNICAL MEMORANDUM.** Scientific and technical findings that are preliminary or of specialized interest, e.g., quick release reports, working papers, and bibliographies that contain minimal annotation. Does not contain extensive analysis.
- **CONTRACTOR REPORT.** Scientific and technical findings by NASA-sponsored contractors and grantees.

- **CONFERENCE PUBLICATION.** Collected papers from scientific and technical conferences, symposia, seminars, or other meetings sponsored or cosponsored by NASA.
- **SPECIAL PUBLICATION.** Scientific, technical, or historical information from NASA programs, projects, and missions, often concerned with subjects having substantial public interest.
- **TECHNICAL TRANSLATION.** English-language translations of foreign scientific and technical material pertinent to NASA's mission.

Specialized services also include creating custom thesauri, building customized databases, organizing and publishing research results.

For more information about the NASA STI program, see the following:

- Access the NASA STI program home page at <http://www.sti.nasa.gov>
- E-mail your question via the Internet to [help@sti.nasa.gov](mailto:help@sti.nasa.gov)
- Fax your question to the NASA STI Help Desk at 443-757-5803
- Telephone the NASA STI Help Desk at 443-757-5802
- Write to:  
NASA Center for AeroSpace Information (CASTI)  
7115 Standard Drive  
Hanover, MD 21076-1320



# Improvements in Modeling 90° Bleed Holes for Supersonic Inlets

*John W. Slater*  
*Glenn Research Center, Cleveland, Ohio*

Prepared for the  
47th Aerospace Sciences Meeting and Exhibit  
sponsored by the American Institute of Aeronautics and Astronautics  
Orlando, Florida, January 5–8, 2009

National Aeronautics and  
Space Administration

Glenn Research Center  
Cleveland, Ohio 44135

## **Acknowledgments**

The author would like to acknowledge the support of the Supersonics Project under the NASA Fundamental Aeronautics Program.

This work was sponsored by the Fundamental Aeronautics Program at the NASA Glenn Research Center.

*Level of Review:* This material has been technically reviewed by technical management.

Available from

NASA Center for Aerospace Information  
7115 Standard Drive  
Hanover, MD 21076-1320

National Technical Information Service  
5285 Port Royal Road  
Springfield, VA 22161

Available electronically at <http://gltrs.grc.nasa.gov>

# Improvements in Modeling 90° Bleed Holes for Supersonic Inlets

John W. Slater  
National Aeronautics and Space Administration  
Glenn Research Center  
Cleveland, Ohio 44135

## Summary

The modeling of porous bleed regions as boundary conditions in computational fluid dynamics (CFD) simulations of supersonic inlet flows has been improved through a scaling of sonic flow coefficient data for 90° bleed holes. The scaling removed the Mach number as a factor in computing the sonic flow coefficient and allowed the data to be fitted with a quadratic equation, with the only factor being the ratio of the plenum static pressure to the surface static pressure. The implementation of the bleed model into the Wind-US CFD flow solver was simplified by no longer requiring the evaluation of the flow properties at the boundary-layer edge. The quadratic equation can be extrapolated to allow the modeling of small amounts of blowing, which can exist when recirculation of the bleed flow occurs within the bleed region. The improved accuracy of the bleed model was demonstrated through CFD simulations of bleed regions on a flat plate in supersonic flow with and without an impinging oblique shock. The bleed model demonstrated good agreement with experimental data and three-dimensional CFD simulations of bleed holes.

## Nomenclature

$A$	area
$A_{\text{bleed}}$	area of bleed hole openings
$A_{\text{region}}$	inlet surface area containing bleed holes
$D$	diameter of the bleed hole
$\gamma$	ratio of specific heats
$L$	length of the bleed hole
$M$	Mach number
$\Phi$	bleed region porosity, $\Phi = A_{\text{bleed}}/A_{\text{region}}$
$p$	pressure
$p_{\text{plenum}}/p_B$	plenum static pressure ratio
$p_{\text{plenum}}/p_{t\delta}$	plenum total pressure ratio
$Q_{\text{sonic}}$	sonic flow coefficient
$Q_{\text{sonic-B}}$	surface sonic flow coefficient
$\rho$	density
$R$	gas constant
$T$	temperature
$v$	velocity component
$W$	rate of flow
$W_{\text{bleed}}$	rate of flow through the bleed region
$W_{\text{sonic}}$	sonic rate of flow based on total conditions
$W_{\text{sonic-B}}$	sonic rate of flow based on surface static conditions

## Subscripts

$B$	property evaluated at the inlet surface (boundary)
$\delta$	property evaluated at the boundary-layer edge
$N$	normal
plenum	property evaluated in the plenum
$t$	total condition

## Introduction

The aerodynamic design of inlets for supersonic flight has commonly included the use of porous bleed regions to reduce the adverse effects of shock/boundary-layer interactions and to enhance the stability of the shock system (Refs. 1 to 10). These bleed regions can consist of hundreds of small holes through which a portion of the low-momentum flow of the inlet boundary layer is extracted. This feature enhances the ability of the boundary layer to withstand the adverse pressure gradient and reduces the likelihood of boundary layer separation (Refs. 4 to 6). The bleed system can also help to remove excess flow to improve matching of flow rates between the inlet and engine (Refs. 9 and 10). This feature is important for stabilizing normal shocks near the throat of the inlet. The bleed flow is extracted by suction into a plenum and then either ducted for use by other aircraft systems or dumped overboard. While porous bleed has benefits, it requires a more complex and heavier inlet and can increase drag (Ref. 1 to 3). The effective use of porous bleed requires careful design of the location and flow rates for the bleed regions.

The methods of computational fluid dynamics (CFD) have been applied to the aerodynamic analysis of supersonic inlet flows containing bleed regions (Refs. 11 to 13). The small scale of the bleed holes results in the typical approach of modeling the effects of porous bleed through the use of surface boundary conditions. Various bleed boundary condition models have been reported by many researchers (Refs. 14 to 22). These models follow the general approach of assuming the bleed region to be a continuously porous surface. The solution points located within the bleed region are computed as boundary conditions in which the local bleed rates and velocity components are computed. The individual bleed holes are not identified nor are the details of the flow within the bleed holes computed. The models attempt to capture the collective behavior of the bleed holes.

The bleed model of Mayer and Paynter (Ref. 17) stands out as representing the current state of porous bleed modeling. This model was implemented within the Wind-US CFD code (Ref. 23). The inlet analyses of Reference 13 illustrate the use of this bleed model for a supersonic inlet analysis. The model allows the bleed rate to vary across the bleed region according to local conditions. This is important when shockwaves are interacting with the bleed region. For example, behind the shockwave, the static pressures are greater, which should result in a greater amount of bleed flow than ahead of the shock. The local bleed rate is calculated by extracting flow properties from the flow field and using a table lookup of empirically based sonic flow coefficients,  $Q_{\text{sonic}}$ . The use of the  $Q_{\text{sonic}}$  data for the bleed model requires the CFD code to compute the Mach number, total pressure, and total temperature at the edge of the boundary layer. However, it may be computationally complex and time-consuming to locate each grid point at the boundary-layer edge, and can be especially difficult for unstructured-grid CFD codes. Furthermore, the edge of the boundary layer may not be well defined, such as in the case of a shock/boundary-layer interaction with extensive boundary-layer separation. Thus, a different approach for using the  $Q_{\text{sonic}}$  data is needed.

The current work improves on the Mayer-Paynter bleed model by introducing a scaling of the  $Q_{\text{sonic}}$  data for 90° bleed holes. The scaling is able to collapse the  $Q_{\text{sonic}}$  data for various Mach numbers to a trend that can then be fitted with a quadratic polynomial, which is only a function of the ratio of plenum static pressure to the surface static pressure. The scaling eliminates the requirement to compute the flow properties at the edge of the boundary layer. The curve fit also provides a rudimentary model for blowing

within a bleed region, which can occur if there is recirculation within the bleed region in the presence of a shock. The next section discusses the bleed modeling and the scaling of the  $Q_{\text{sonic}}$  data. The improved bleed model was implemented into the Wind-US CFD code.

The improved bleed model was demonstrated for flows over bleed regions on flat plates with and without shocks for which experimental data was available for comparison. The bleed model was also compared to three-dimensional CFD simulations of the flow through the bleed holes and plenum. Such simulations can provide details on the bleed flow useful for improving the bleed models. These simulations include a single bleed hole in uniform flow and a series of bleed holes interacting with an oblique shock.

## Improved Porous Bleed Boundary Condition Model

The porous bleed boundary condition is imposed for surface grid points located within the bleed region. The model assumes the region is continuously porous, and so, the flow through individual holes is not resolved nor are individual holes recognized. The cross-sectional area of the bleed holes  $A_{\text{bleed}}$  is represented by the porosity  $\Phi$  in the form of

$$A_{\text{bleed}} = \Phi A_{\text{region}} \quad (1)$$

where  $A_{\text{region}}$  is the surface area of the bleed region. The ability of the bleed holes to extract bleed flow is represented by the sonic flow coefficient  $Q_{\text{sonic}}$ . The bleed flow rate is calculated in the form of

$$W_{\text{bleed}} = Q_{\text{sonic}} W_{\text{sonic}} \quad (2)$$

The  $W$  is the flow rate given in the general form of

$$W = \rho A v = p_t A M \left( \frac{\gamma}{RT_t} \right)^{1/2} \left( 1 + \frac{\gamma-1}{2} M^2 \right)^{-(\gamma+1)/2(\gamma-1)} \quad (3)$$

The  $W_{\text{sonic}}$  is a reference flow rate defined as

$$W_{\text{sonic}} = \Phi A_{\text{region}} p_t \left( \frac{\gamma}{RT_t} \right)^{1/2} \left( \frac{\gamma+1}{2} \right)^{-(\gamma+1)/2(\gamma-1)} \quad (4)$$

The  $W_{\text{sonic}}$  is calculated by assuming isentropic conditions through the bleed holes with sonic flow ( $M = 1$ ) within the bleed holes.

The bleed boundary condition requires  $Q_{\text{sonic}}$  to be evaluated. The approach of Mayer and Paynter (Ref. 11) was to use a table lookup of empirical data. The data table was specific for a given bleed hole configuration (hole angle, diameter ( $D$ ), and length ( $L$ )). The data for  $90^\circ$  holes was based on data used by Syberg and Hickox (Ref. 2) for holes with a hole length-to-diameter ratio,  $L/D = 3$ . The values of  $Q_{\text{sonic}}$  were for various Mach numbers from 0 to 1.9. At each Mach number, the  $Q_{\text{sonic}}$  varied with respect to the ratio between the plenum static pressure and the total pressure of the inlet flow at the edge of the approaching boundary layer,  $p_{\text{plenum}}/p_{t0}$ . The total pressure and total temperature at the edge of the boundary layer above the bleed region were used in Equation (4).

Other data sets exist for  $Q_{\text{sonic}}$  that could be used for the bleed boundary condition. McLafferty and Ranard (Ref. 24) provided some of the earliest data. Willis, Davis, and Hingst (Ref. 25) provided a more recent and excellent data set. These data sets assumed the bleed region to be continuously porous and defined  $Q_{\text{sonic}}$  using Equation (2) with  $W_{\text{bleed}}$  measured and  $W_{\text{sonic}}$  computed using Equation (4). The total pressure and total temperature of Equation (4) were measured at the edge of the boundary layer approaching the bleed region.

Willis, Davis, and Hingst (Ref. 25) illustrated the characteristics of  $Q_{\text{sonic}}$  and formed the basis of data scaling for an improved bleed model. The experiments of Willis, Davis, and Hingst measured bleed flow through a series of flat plates, each containing a porous bleed region. The plates varied by hole angle, hole length, and hole entry shape. Here we consider plate C1 with circular bleed holes at an angle of  $90^\circ$  to the plate surface. The bleed region contained 6 rows, containing 12 bleed holes in each row over a streamwise distance of 2.75 in. and a width of 7.0 in. The holes had diameter of  $D = 0.25$  in. and  $L/D = 1.0$ . The porosity was  $\Phi = 19.1$  percent. The plates were mounted flush onto one side of the test section of the 1- by 1-Foot Supersonic Wind Tunnel at the NASA Glenn Research Center. The boundary layer over the plate was the naturally occurring boundary layer on the sides of the wind tunnel. Fences at the sides of the bleed region isolated the bleed region from the tunnel wall boundary layers. The flow conditions and boundary-layer profile approaching the bleed region were measured with a translating pitot probe and wall static-pressure taps at a reference location 3.225 in. ahead of the bleed region. The bleed plenum was attached to the outside of the wind tunnel with ducting to an altitude exhaust. A mass flow plug was used to establish the bleed flow rate, which was measured using a calibrated nozzle. The experiment also examined the boundary layer downstream of the bleed region (Ref. 26). The uncertainty of the experimental data was reported as 0.007 psi for static pressures, 0.045 psi for total pressures, and 2.4 percent for values of  $Q_{\text{sonic}}$ .

Figure 1 shows the  $Q_{\text{sonic}}$  data collected for plate C1 at approach flow Mach numbers 1.27, 1.58, 1.98, and 2.46. The abscissa of the data is the plenum total pressure ratio, which is the ratio of the plenum static pressure to the total pressure at the edge of the approaching boundary layer ( $p_{\text{plenum}}/p_{t\delta}$ ). For each Mach number, the  $Q_{\text{sonic}}$  and the bleed flow  $W_{\text{bleed}}$  increase as the plenum total pressure ratio is reduced. At some ratio, the bleed holes choke, and a maximum bleed rate is achieved. Figure 1 illustrates the decrease in  $Q_{\text{sonic}}$  as the Mach number increases. This decrease reflects the increased losses and difficulty in bleeding the flow as the Mach number increases. The change in  $Q_{\text{sonic}}$  with increased Mach number is greater between Mach 1.27 and 1.58 than between Mach numbers 1.98 and 2.46.

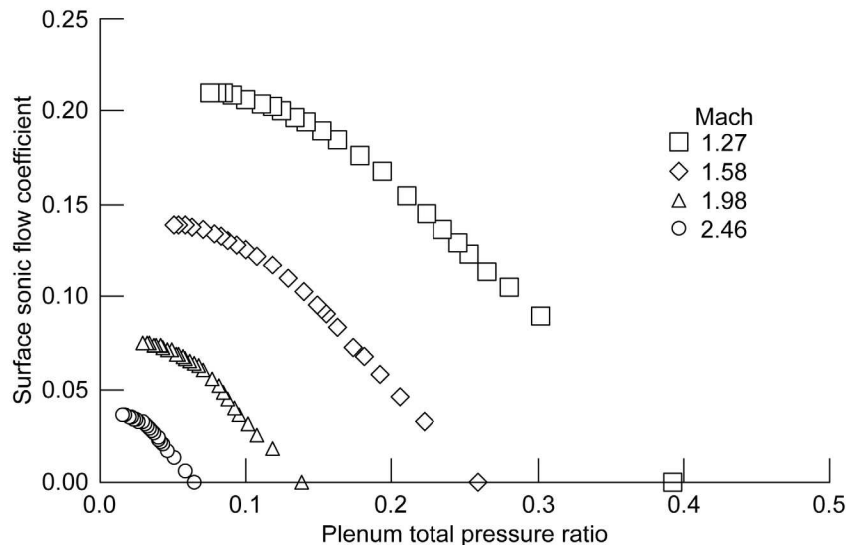


Figure 1.—The sonic flow coefficient data for plate C1 with  $90^\circ$  holes (Ref. 5).

Within a CFD code, the bleed boundary condition is imposed on the surface solution points located within the bleed regions at the boundaries of the flow domain. At each solution point, Equations (2) and (4) are evaluated. The  $A_{\text{region}}$  for Equation (4) is the cell surface area about the boundary solution point  $A_B$ . In the previous bleed model, the CFD code would evaluate the Mach number, total pressure, and total temperature at the edge of the boundary layer to look up the value of  $Q_{\text{sonic}}$  for Equation (2) using Figure 1, and would also provide the total pressure and temperature for Equation (4). The bleed through the boundary cell area  $W_{\text{bleed}}$  was calculated using Equation (2). The normal component of the velocity was then evaluated as

$$v_N = \frac{W_{\text{bleed}}}{\rho_B A_B} \quad (5)$$

Thus, the effect of bleed at a surface solution point is imposed through the normal component of the surface velocity as calculated by Equation (5). A tangential component of velocity may be significant, but is not modeled (Ref. 27). Furthermore, for certain bleed rates, the bleed can impose a roughness onto the flow that may be important for turbulence quantities of the turbulence models (Ref. 16). Both these factors are topics of future research to enhance the bleed model.

The bleed model described above has some drawbacks for CFD simulations. First, locating the boundary-layer edge above a surface solution point in the bleed region may be a complex task for the CFD code. One approach is to estimate the boundary layer thickness and determine the grid point at that distance from the surface. For structured grids, one can indicate the number of grid points from the wall and follow a grid line from the boundary point out into the flow field. For unstructured grids, a search algorithm would be needed because grid points do not follow a structured order away from the wall. A second concern is that the edge of the boundary layer may not be well defined. Bleed is often desirable in regions of shock/boundary-layer interactions, but these flow fields may contain regions of separated flows and distorted flow in a range of Mach numbers. Defining a boundary-layer edge may not be possible for such flow fields.

This concept raises the question as to whether surface conditions near the bleed holes can be used to characterize the bleed data, rather than referencing the data to the conditions of the approaching boundary layer. A new scaling of the bleed data attempts to characterize the bleed data with respect to surface conditions. The new scaling is similar to that proposed by Davis (Ref. 28, unpublished); however, the new scaling is not based on a curve fit of the data and removes the Mach number at the edge of the boundary layer as a factor. The new scaling considers an alternative reference flow for the sonic flow coefficient of the form

$$W_{\text{sonic-B}} = \Phi A_{\text{region}} p_B \left( \frac{\gamma}{RT_B} \right)^{1/2} \left( \frac{\gamma+1}{2} \right)^{-(\gamma+1)/2 (\gamma-1)} \quad (6)$$

The total conditions are replaced with the static pressure and temperature at the inlet surface local to the bleed hole. The subscript  $B$  denotes the surface or boundary value. The static pressure and temperature are both easily obtained in a CFD flow field.

The surface sonic flow coefficient can be defined as

$$Q_{\text{sonic-B}} = \frac{W_{\text{bleed}}}{W_{\text{sonic-B}}} = \frac{W_{\text{bleed}}}{W_{\text{sonic}}} \left( \frac{W_{\text{sonic}}}{W_{\text{sonic-B}}} \right) \quad (7)$$

The quantity in the parenthesis of Equation (7) can be evaluated using Equations (4) and (6) with the result of

$$Q_{\text{sonic-B}} = Q_{\text{sonic}} \left( \frac{p_{t\delta}}{p_B} \right) \left( \frac{T_B}{T_{t\delta}} \right)^{1/2} \quad (8)$$

The assumptions can be made that

$$\frac{p_{t\delta}}{p_B} = \left( 1 + \frac{\gamma-1}{2} M_\delta^2 \right)^{\gamma/(\gamma-1)} \quad \text{and} \quad \left( \frac{T_B}{T_{t\delta}} \right)^{1/2} \approx 1 \quad (9)$$

The second assumption of Equation (9) could be modified to account for recovery for an adiabatic wall temperature (Ref. 29), which will be the topic of future research efforts.

The scaling can be performed through the operations

$$Q_{\text{sonic-B}} = Q_{\text{sonic}} \left( \frac{p_{t\delta}}{p_B} \right) \quad (10)$$

and

$$\frac{p_{\text{plenum}}}{p_B} = \frac{p_{\text{plenum}}}{p_{t\delta}} \left( \frac{p_{t\delta}}{p_B} \right) \quad (11)$$

Figure 2 shows the effect of the scaling the sonic flow coefficient data presented in Figure 1. The scaled data collapse along a trend such that the surface sonic flow coefficient only varies with respect to the static plenum pressure ratio ( $p_{\text{plenum}}/p_B$ ). The Mach number at the boundary-layer edge has been removed as a factor. The bleed flow for the new bleed model can be calculated as

$$W_{\text{bleed}} = Q_{\text{sonic-B}} W_{\text{sonic-B}} \quad (12)$$

Both terms of the right-hand side of Equation (12) are evaluated from the plenum static pressure ratio. The plenum static pressure is either specified or computed based on other conditions, such as those discussed in Reference 22 for a bleed plenum with a fixed-area plenum exit.

### Curve Fit of the Scaled Data

A quadratic curve was fitted to the scaled data of Figure 2. The quadratic equation is

$$Q_{\text{sonic-B}} = -0.59361420 \left( \frac{p_{\text{plenum}}}{p_B} \right)^2 + 0.03069346 \left( \frac{p_{\text{plenum}}}{p_B} \right) + 0.59799735 \quad (13)$$

Figure 2 indicates that at a static pressure ratio of approximately 1.03, the bleed flow is zero. The plenum pressure is slightly higher than the surface static pressure. This fact may indicate a dynamic or ram effect of the flow into the bleed holes, even at 90°. As the static pressure ratio approaches zero, the surface sonic flow coefficient approaches 0.6, which reflects the loss incurred in turning the flow into the bleed hole.

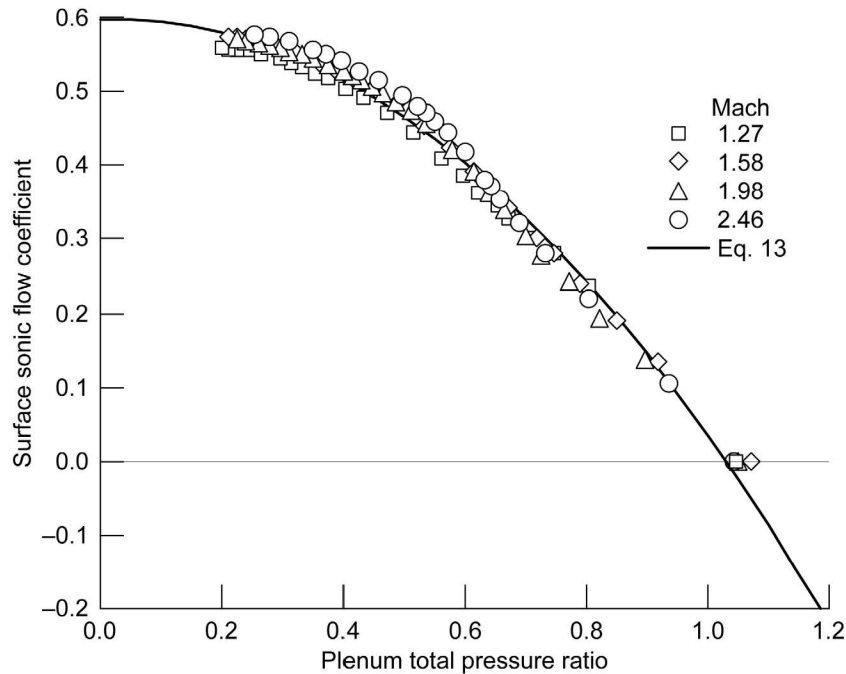


Figure 2.—The surface sonic flow coefficient data plotted with the quadratic fit of the data (Eq. 13).

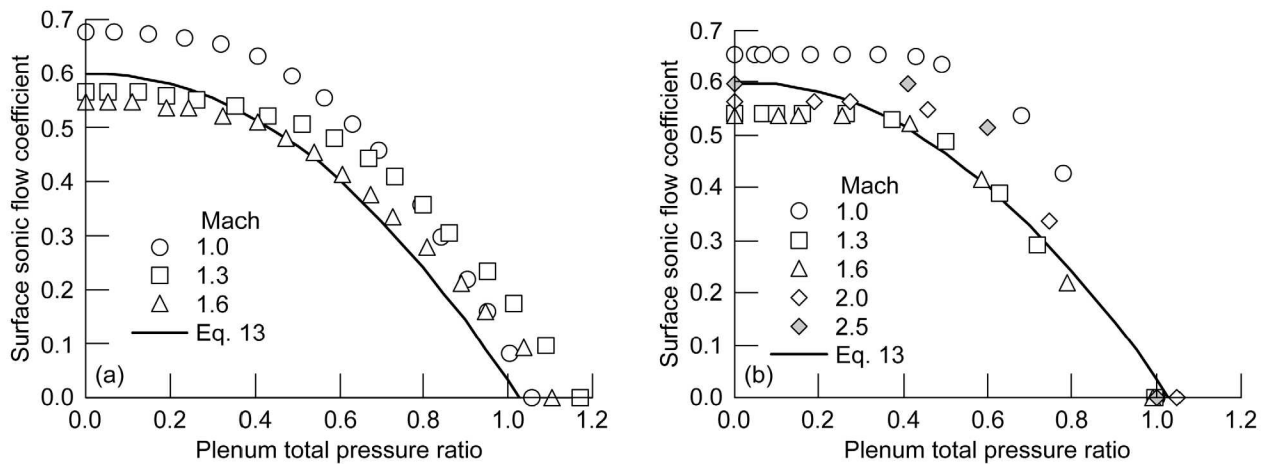


Figure 3.—The scaling applied to the sonic flow coefficient data sets. (a) From Syberg and Hickox (Ref. 2). (b) From Mayer and Paynter (Ref. 17).

Figure 3 shows the application of the scaling to sonic flow coefficient data sets used in References 2 and 17. There is greater variation in the scaled values than shown in Figure 2, but the curve fit of Equation (13) does well in characterizing the data. The exception is the data for Mach 1.0 where the curve fit indicates lower values for the surface sonic flow coefficient. Note that the minimum Mach number of Figure 1 upon which the curve fit was generated was Mach 1.27. The comparisons of Figure 3 suggest that the curve fit may not work well for characterizing bleed rates below Mach 1.27. Given that most of the flow in supersonic inlets is above Mach 1.27, the curve fit should provide a good characterization of the bleed flow in supersonic inlets.

An additional benefit of the scaling of the sonic flow coefficient as expressed in Equation (13) is that it provides a rudimentary model for blowing in a bleed hole. When the static pressure ratio is greater than

1.03, the value of the surface sonic flow coefficient is negative, which by Equation (2) will result in a negative bleed flow or blowing. While large amounts of blowing are not intended in the design of a supersonic inlet, it is possible to experience recirculation within a bleed region. Recirculation can occur when a shockwave is interacting with the bleed region, and the total bleed flow for the bleed region is small. The high pressures downstream of the shock cause pressurization of the bleed plenum, which forces the bleed plenum to blow flow out the bleed holes upstream of the shock where the local pressures are lower.

## CFD Simulation of Bleed Flows

Several CFD simulations of flow fields with porous bleed illustrate the features of bleed flows and demonstrate, verify, and validate the improvements in the bleed modeling of 90° bleed holes. The simulations of this report used the Wind-US CFD code (Ref. 23). Wind-US solves the Reynolds-averaged Navier-Stokes equations for turbulent, compressible flows using a cell-vertex, finite-volume, time-marching approach. The cell-face fluxes are computed using a second-order, Roe flux difference-splitting, upwind-biased formulation. Steady flows are solved in a time-dependent manner using a first-order, Euler implicit method with local time stepping. The simulations were performed using multiblock, structured grids, and the one-equation Spalart-Allmaras (S-A) and/or the two-equation Menter shear stress transport (SST) turbulence model.

### Porous Bleed on a Flat Plate in Uniform Supersonic Flow

This bleed flow involved uniform supersonic flow over a flat plate containing a porous bleed region. This flow was studied in wind tunnel tests conducted by Willis, Davis, and Hingst at the NASA Glenn Research Center in the early 1990s (Refs. 25 and 26). The primary objective of the wind tunnel study was to examine the effect of bleed hole geometry parameters on the bleed rates (Ref. 25) and the downstream boundary layer (Ref. 26). This wind tunnel study provided the data in Figure 1. For the present work, CFD simulations were performed for a two-dimensional flow domain using the bleed boundary condition. The objective was to verify that accurate bleed rates could be obtained from the CFD methods. Hamad and Li studied bleed flow using CFD methods with a three-dimensional flow domain that included the bleed holes and plenum (Ref. 30).

The CFD-simulated bleed plate C1 is described in the Improved Porous Bleed Boundary Condition Model section. The CFD simulations were performed at Mach numbers 1.27, 1.58, 1.98, and 2.46. Figure 4 shows the computational flow domain used for the two-dimensional CFD simulations. The inflow boundary was located at  $x = 0.0$  in. and was specified with fixed-flow properties for a supersonic inflow. The inflow properties were generated by separate CFD simulations of a flat plate that generated a boundary layer matching the properties of the approach boundary layer at the reference location. The approaching Mach number, total pressure, and total temperature were computed at the edge of the approaching boundary layer. The plate and bleed region were at the bottom of the flow domain. The bleed region extended from  $x = 4.0$  to 6.75 in. and is shown with momentum vectors indicating the bleed flow. The bleed boundary condition was used within the bleed region and adiabatic, no-slip boundary conditions were used on the rest of the plate. The top of the flow domain was the center plane of the tunnel, and an inviscid boundary condition was applied. The right boundary of the flow domain was a supersonic outflow boundary, and first-order extrapolation was used for the boundary condition.

A single-block, structured H-grid was used for the flow domain. A grid convergence study determined the appropriate grid spacing required to resolve the grid-independent bleed flow rate. Three grids were generated that had streamwise grid spacing within the bleed region of  $0.8D$ ,  $0.4D$ , and  $0.2D$ , creating a coarse, medium, and fine grid, respectively. The wall spacing at the adiabatic, no-slip boundary was specified at a nondimensional wall spacing of  $y^+ = 4$  at Mach 1.27 to  $y^+ = 2$  for Mach 2.46. The spacing at the inflow, outflow, and top boundaries matched those of the streamwise spacing within the bleed region. A hyperbolic tangent method was used to distribute the grid points in each direction. An

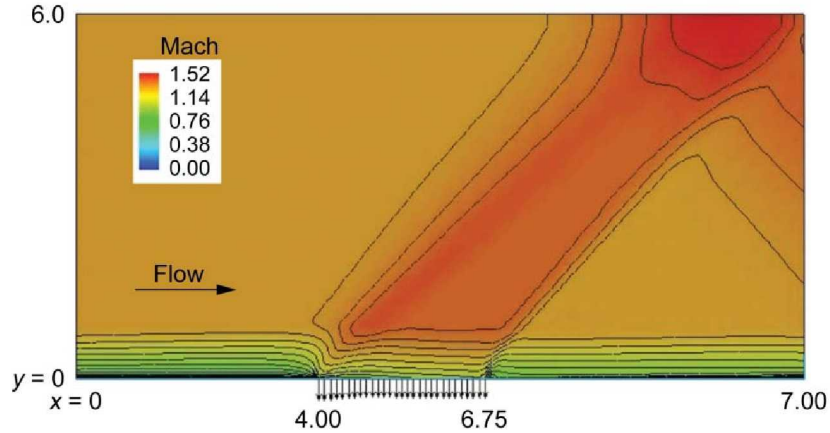


Figure 4.—Flow domain, Mach number contours, and bleed momentum vectors for Mach 1.27 flow over a porous bleed region on a flat plate.

algebraic method was used to generate the two-dimensional interior grid. The resulting grid sizes were 53 by 61, 89 by 115, and 193 by 203. CFD simulations were performed for the three levels of grid at the four Mach numbers and for a plenum static pressure of 2.0 psi. Table I shows the results for the sonic flow coefficient for the three grids for the Mach 1.27 simulations. The medium grid with a resolution of  $0.4D$  seemed to provide adequate resolution of the bleed flow rate. This grid was used for the remaining CFD simulations. The initial flow field for the simulations was the freestream conditions with the inflow conditions interpolated from the boundary-layer solution. Iterative convergence was examined by monitoring the bleed flow rate.

TABLE I.—GRID CONVERGENCE FOR MACH 1.27 FLOW OVER A POROUS BLEED REGION

$\Delta s$ , in.	$\Delta s/D$	Grid size	$Q_{\text{sonic}}$	$ Q_{\text{sonic}} $ , percent
0.2	0.8	53 by 61	0.1757	5.13
0.1	0.4	89 by 115	0.1700	1.67
0.05	0.2	193 by 203	0.1672	----

Figure 4 shows the typical flow field; the flow field is for the Mach 1.27 simulation, with the bleed flow at its maximum rate. The bleed flow across the bleed region was fairly uniform, indicated by arrows representing the bleed flow momentum vectors. The bleed caused a localized expansion and acceleration of the flow at the start of the bleed as the core flow was turned into the bleed region. For the Mach 1.27 approach flow, Mach number reached a peak of  $M_{\delta} = 1.42$  at the start of the bleed region with values of  $M_{\delta} = 1.38$  over the aft two-thirds of the bleed region. At the end of the bleed region, the flow turned back parallel to the wall, and a weak shock was formed, reducing the Mach number back to  $M_{\delta} = 1.27$ . The expansion and shockwaves reflected off the top boundary of the flow domain, but this did not affect the bleed flow.

The variations of  $Q_{\text{sonic}}$  with the plenum total pressure ratio ( $p_{\text{plenum}}/p_{t\delta}$ ) are shown in Figure 5 for the four Mach numbers. The error bars for the experimental uncertainty in the measurement of  $Q_{\text{sonic}}$  are plotted. Overall, the simulations did well in matching the data. The solid symbols denote the CFD results using the old bleed model as presented in Reference 22. The open symbols show the results for the new bleed model that used the curve fit for the surface sonic flow coefficient of Equation (13). Some distinct improvements can be seen from using the new bleed model.

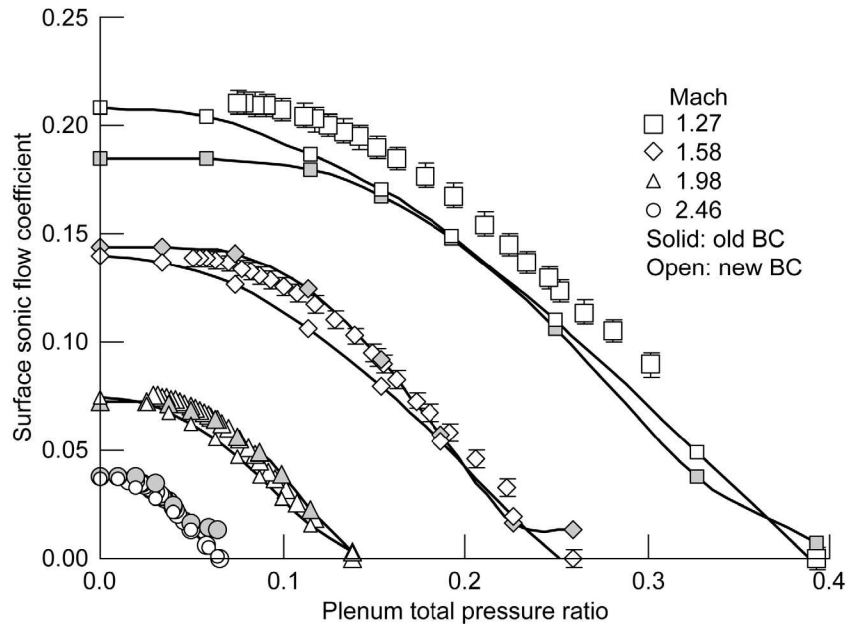


Figure 5.—The sonic flow coefficients for bleed on a flat plate in a uniform, supersonic flow (Ref. 25).

The new model provides a smoother variation of the bleed rates as the sonic flow coefficient approaches zero, and the total pressure ratios for zero sonic flow coefficients show an improved match with the experimental data. Much of this improvement is due to the smooth variation of Equation (13) as the sonic flow coefficient approaches zero. The old bleed model used a table lookup of the sonic flow coefficient that exhibited discontinuous behavior as the sonic flow coefficient approached zero. This behavior is most noticeable in the plot of data of the old model for Mach 1.58.

As the total pressure ratio decreases and the sonic flow coefficients approach their maximum value, the results of the old and new bleed models are similar for Mach numbers of 1.58, 1.98, and 2.46. At Mach 1.27, the new model shows an improvement in matching the maximum sonic flow coefficient than for the old model. In Reference 22 it was proposed that the old model was looking at the edge of the boundary layer and observing a higher Mach number (Mach 1.38 to 1.42) because of the expansion above the bleed region. The higher Mach number would result in the table lookup indicating a lower  $Q_{\text{sonic}}$ . The new boundary condition no longer looks at the edge of the boundary layer, but rather the local conditions and is able to yield the  $Q_{\text{sonic}}$  values closer to the data.

### Bleed Flow Through a Single Bleed Hole in Uniform Supersonic Flow

The bleed flow through a single bleed hole in uniform supersonic flow was studied in wind tunnel tests conducted by Bodner, et al. at the NASA Glenn Research Center in the mid 1990s (Refs. 31 and 32). For the present work, CFD simulations included the bleed hole and plenum into the CFD simulation flow domain. Such CFD simulations have yielded significant information on the detailed shock structures and flow physics within bleed holes (Refs. 21, 27, 33, and 36). Such information can provide significant insights for developing bleed models. The CFD simulations provide a verification of the bleed model.

The CFD simulations involved a single 90° bleed hole with a diameter  $D = 0.236$  in. and length of  $L = 2D$ . The hole was located in a disk mounted flush with the bottom of the test section of the 15- by 15-cm wind tunnel at the NASA Glenn Research Center. The boundary layer over the plate was the naturally occurring boundary layer on the bottom surface of the wind tunnel. The flow conditions and boundary layer profile approaching the bleed region were measured with a translating pitot probe and wall static pressure ports. The reference station for the approach flow was located 2.46 in. ahead of the

center of the bleed hole. The bleed plenum was attached to the outside of the wind tunnel with ducting to a vacuum exhaust. The plenum was cylindrical with an inside diameter of 2.874 in. and an axial length of 3.50 in. The axis of the plenum was parallel to the axis of the bleed hole. A vacuum chamber established the bleed flow rate, which was measured using a calibrated nozzle. The uncertainty of the experimental data was reported as  $\pm 1.5$  percent for total pressures, and  $\pm 1$  percent for values of  $Q_{\text{sonic}}$ .

The CFD simulations were performed at a Mach number of 2.46. Figure 6 shows the side view and front view of the computational flow domain. The bleed hole and plenum are located below the tunnel, shown at the bottom of Figure 6. Geometric and flow symmetry were assumed and allowed only half of the tunnel, bleed hole, and plenum to be simulated. A reflection boundary condition was used on the symmetry plane. The bottom and side of the tunnel were specified with adiabatic, no-slip boundary conditions. The top of the tunnel was specified as an inviscid wall to require less grid points to resolve the boundary layer, which was assumed not to influence the flow through the bleed hole. The inflow boundary was positioned an axial distance of 38.46 in. ahead of the center axis of the hole. This position provides a turbulent boundary layer at the reference location that matched the reference boundary-layer profile and edge conditions of the experiment. The conditions at the boundary-layer edge were a Mach number of 2.46, total pressure of 25.0 psia, and a Reynolds number of  $5.15 \times 10^6/\text{ft}$ . The boundary-layer thickness was 0.5079 in. The outflow boundary was positioned 5.0 in. downstream of the center axis of the bleed hole, and a first-order extrapolation boundary condition was used for the supersonic outflow. The plenum was modeled as a cylinder with a converging-diverging nozzle directed downward for the outflow for the plenum. The exit for the plenum nozzle was located 6.472 in. below the bottom wall of the tunnel, and a subsonic outflow boundary condition was imposed, with a specified static pressure. The bleed flow reached very low speeds within the plenum, and the intent of the nozzle was to create a smooth exit for the bleed flow from the plenum. The walls of the plenum and bleed hole were specified as adiabatic, no-slip boundary conditions.

A structured grid with 12 blocks was generated for the flow domain. The grids across the blocks abutted and matched contiguously. The bleed hole consisted on a single cylindrical grid block with a singular axis down the center of the hole. Similarly, the bleed plenum and nozzle consisted of cylindrical grid blocks with singular axes. Figure 7 shows the grid on the bottom of the tunnel about the bleed hole. Cylindrical grids about the hole match up to H-grids for the tunnel. The grids are clustered at the no-slip walls. Initial solutions for the tunnel boundary layer indicated that a wall spacing of  $2.4 \times 10^{-4}$  in. provided a nondimensional wall spacing of  $y^+ \approx 1.0$ . The grid distribution was determined using a hyperbolic tangent method with end spacings specified. The number of grid points along an edge was selected such that the maximum grid stretching was less than 15 percent. Within the bleed hole, the maximum spacing was limited to 0.005 in. ( $0.02D$ ), which set the level of maximum resolution of the flow within the bleed hole. This grid established the highest resolution of the flow field for the grid convergence study (fine grid). The resulting grid contained 678 375 grid points within the bleed hole. The entire grid contained over 6.66 million grid points, with over half of the grid points located within 3 diameters of the bleed hole and within the plenum.

The CFD flow solution was initialized with Mach 2.46 flow within the tunnel and very low speed (Mach 0.01) flow within the bleed hole and plenum, with a static pressure equal to the tunnel static pressure. An inviscid boundary condition was imposed at the plenum nozzle exit to initially not allow any bleed flow. This created the zero-bleed solution. Flows with bleed were then simulated by imposing the subsonic outflow boundary condition at the plenum nozzle outflow and specifying reduced values of static pressure to draw out the plenum flow. Subsequently lower values of exit static pressure yielded a sequence of solutions with greater bleed flow until the maximum bleed flow was obtained with essentially a vacuum within the plenum.

At each solution point, the iterative convergence was examined by monitoring the amount of bleed flow and the plenum static pressure. The bleed flow was measured within the plenum nozzle where the flow was entirely directed toward the exit without recirculation, which ensured an accurate evaluation of the mass flow. The plenum pressure was obtained by mass averaging the static pressure on a horizontal plane near the start of the nozzle.

The grid convergence was examined by solving the flow field on three grids of subsequent coarseness. The Wind-US code allows grid sequencing that allows the solution to be computed on coarser grids obtained by skipping a number of grid points. The grid sensitivity study can be conducted without having to generate coarser grids. The medium grid was obtained by skipping every other grid point. The coarse grid was obtained by skipping three grid points. This method can also be used to accelerate convergence by starting the initial solution on the coarse grid. Table II lists the results on the coarse ( $0.08D$ ), medium ( $0.04D$ ), and fine ( $0.02D$ ) grids for both the S-A and Menter SST turbulence models. The simulations were performed with the bleed rate approximately 75 percent of its maximum value. The bleed rates showed little variation between the medium and fine grids, shown in Figure 8, which plots the data of Table II. The value of  $Q_{sonic}$  from the experiment is also plotted.

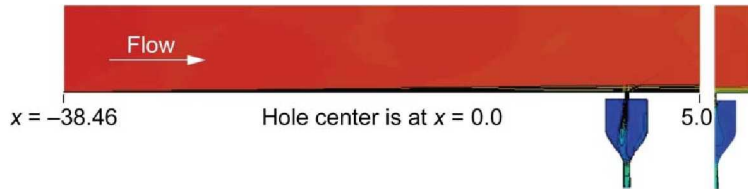


Figure 6.—Side and front views of the flow domain for a single bleed hole.

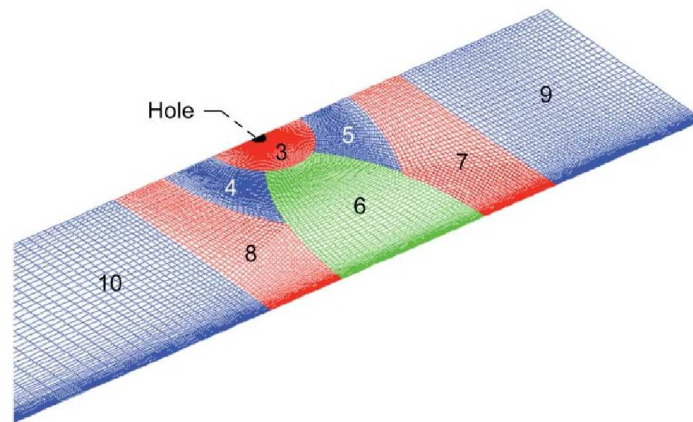


Figure 7.—Grid zones on the tunnel wall about the bleed hole.

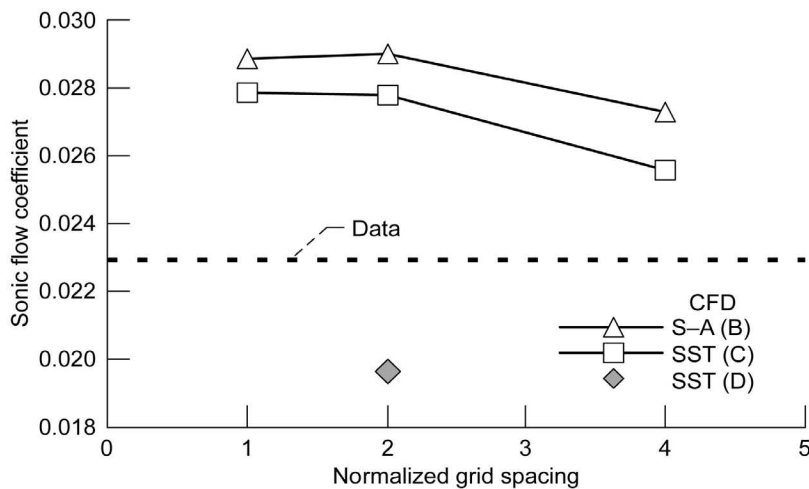


Figure 8.—Grid convergence and turbulence model sensitivity (computational fluid dynamics (CFD), Spalart-Allmaras (S-A), and shear stress transport (SST)).

TABLE II.—GRID CONVERGENCE FOR A SINGLE BLEED HOLE ON A FLAT PLATE

Turbulence model	$\Delta s/D$	Hole grid size	$Q_{\text{sonic}}$	$ Q_{\text{sonic}} $ , percent
S-A	0.08	12 by 51 by 19	0.0273	5.52
	0.04	23 by 101 by 38	0.0290	0.05
	0.02	45 by 201 by 75	0.0289	---
SST	0.08	12 by 51 by 19	0.0256	8.07
	0.04	23 by 101 by 38	0.0278	0.00
	0.02	45 by 201 by 75	0.0278	---

The simulations with the S-A and SST turbulence models are essentially the same with both indicating  $Q_{\text{sonic}}$  values approximately 25 percent higher than the experimental data. However, it was discovered that the approach Mach number for these simulations was only 2.38 rather than 2.46. The inflow conditions were subsequently changed to obtain the correct inflow Mach number of 2.46 for the remaining simulations. Further simulations could be conducted using the medium grid with a resolution of  $0.04D$  using the Menter SST turbulence model. Figure 8 shows the result of simulation D, which was conducted on the medium grid with the Menter SST turbulence model.

Figure 9 shows the Mach number contours of the flow within the bleed hole at the symmetry plane at the maximum flow rate. Figure 10 shows the Mach contours at cross-sectional planes through the bleed hole. Shih, et al. (Ref. 33) provided the first description of the flow within such a bleed hole. The flow approaching the hole is turned into the hole, and this causes an expansion that increases the Mach number above the forward portion of the hole. A shear layer forms from the leading edge of the hole into the hole. The flow impacts the back wall of the hole and forms a two-segment “barrier” shock. One segment is formed by the flow turning at the back wall into the hole, and the other is formed by the portion of the flow being turned as it avoids being drawn into the hole. If the turning angle is great enough, then both segments are detached, forming a small subsonic region. The barrier shock helps turn the flow not captured by the bleed hole back to the static pressure and flow direction of the plate. The flow that enters the hole encounters a fluidic contraction and expansion to form a supersonic jet along the rear surface of the hole. The jet can penetrate supersonically into the plenum several bleed-hole diameters. The flow separates at the forward portion of the hole, forming a region of separated flow. If the hole is long enough, reattachment may occur within the hole. For this flow, the plenum is large enough that the jet eventually dissipates and the flow circulates throughout the plenum at a low speed.

Figure 11 shows the variation of the sonic flow coefficient. Uncertainties in the experimental data are not large enough to show on the symbols of Figure 11. The results of the CFD simulations matched well with the data; the data strongly suggests that CFD simulations can be used to obtain  $Q_{\text{sonic}}$  data for bleed configurations or flow conditions for which experimental data is not available. The plotted curve fit of Equation (13) compared well to the data and CFD simulation. The curve fit was based on experiments with multiple rows of bleed holes. Data suggested that a test or CFD simulation with a single bleed hole can be used to obtain  $Q_{\text{sonic}}$  data. Bodner (Refs. 31 and 32) also noted that the single-hole data compared well to the multiple-hole data of Willis, Davis, and Hingst (Ref. 25) and suggested that perhaps the hole interactions were not significant for that data set for  $90^\circ$  bleed holes.

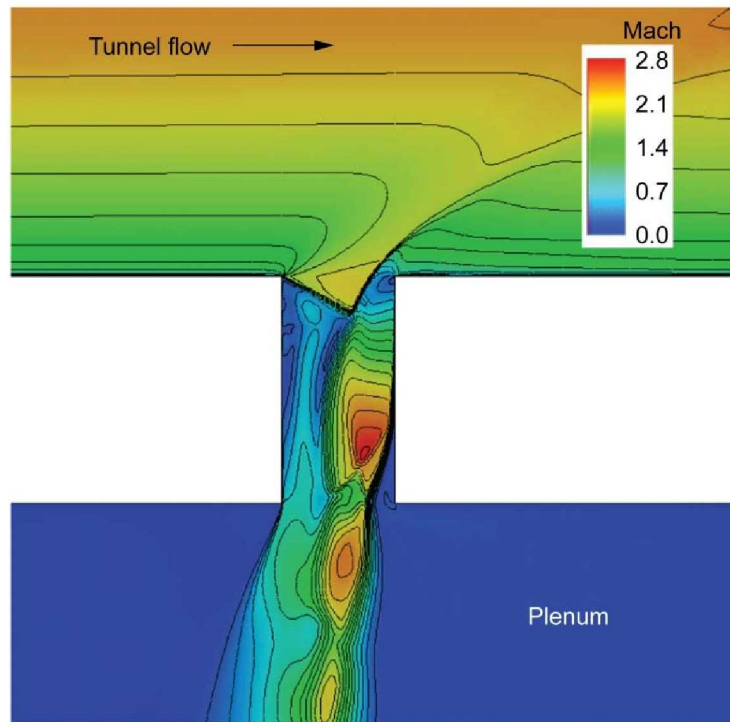


Figure 9.—Mach number contours at the symmetry plane for maximum bleed flow through a single bleed hole.

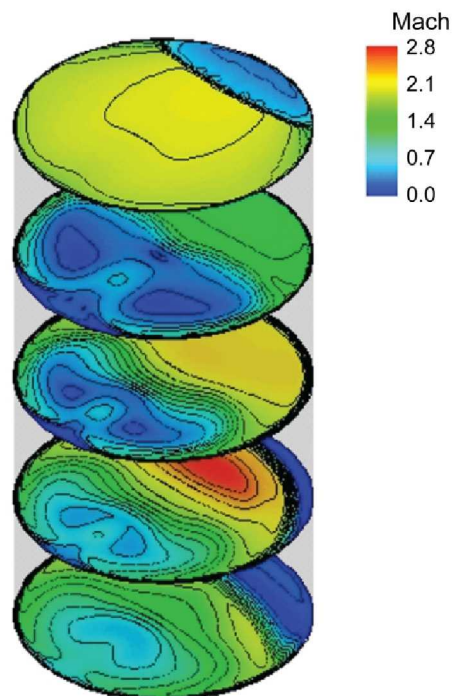


Figure 10.—Mach number on planes within the bleed hole.

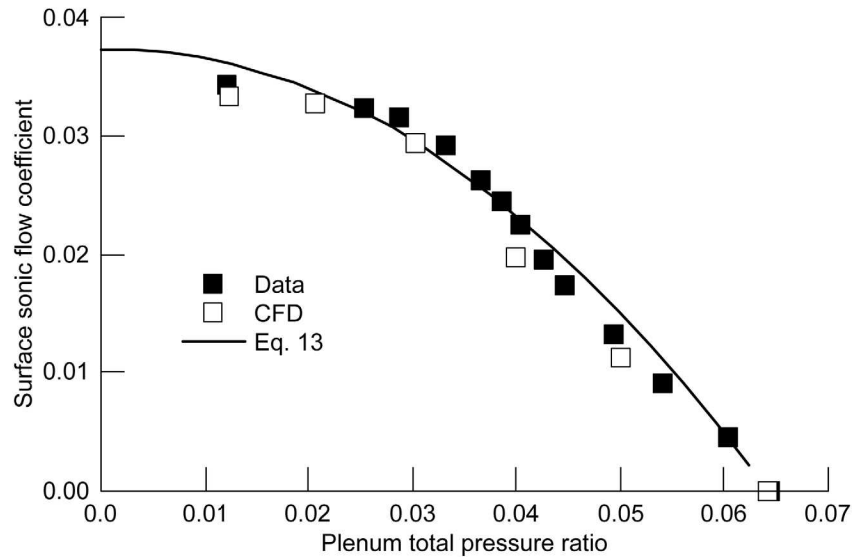


Figure 11.—The sonic flow coefficients for bleed flow through a single bleed hole (Ref. 8) (computational fluid dynamics (CFD)).

### Interaction of an Oblique Shock With a Porous Bleed Region on a Flat Plate

This bleed flow involved the interaction of an oblique shock with a porous bleed region on a flat plate and was studied in wind tunnel tests conducted by Willis, Davis, and Hingst at the NASA Glenn Research Center in the mid-1990s (Ref. 34). The wind tunnel study continued the tests of References 25 and 26, but added a plate to generate the oblique shock. For the present work, CFD simulations included a two-dimensional flow domain using the bleed boundary condition and a three-dimensional flow domain in which the flow through the bleed holes and plenum were included in the flow domain. The objective was to evaluate the ability of CFD methods to simulate bleed in an adverse pressure gradient with the possibility of recirculation within the bleed region. This flow was simulated by previous researchers (Refs. 21, 35, and 36).

For these tests, a total of 8 rows were opened on plate C1, which extended the bleed region a streamwise distance of 3.75 in. The reference station for the approach flow was located 3.225 in. ahead of the start of the bleed region. Based on an inviscid flow analysis, the shock generator was oriented at an 8° incidence to the approach flow and positioned such that oblique shock impinged at the midpoint of the bleed region. The interaction imposed a significant adverse pressure gradient over the bleed region. Without bleed, the turbulent boundary layer contained a small separation zone about the shock impingement point.

The CFD simulations were performed at a Mach number 2.46. The computational flow domain used for the two-dimensional CFD simulations is shown in Figure 12. The inflow boundary at  $x = -15.0$  in. was specified with fixed-flow properties for a supersonic inflow. The inflow properties were generated by separate CFD simulations of a flat plate that generated a boundary layer that matched the properties of the approach boundary layer at the reference location reported from the wind tunnel tests. This required a flat plate of length of 95.0 in. The Mach number at the inflow of the flat plate was 2.50. The boundary-layer edge conditions at the reference location were a Mach number of 2.46, total pressure of 25.0 psia, and a Reynolds number of  $5.52 \times 10^6/\text{ft}$ . The boundary-layer thickness was 1.04 in. The plate and bleed region are at the bottom of the flow domain. The bleed region extends from  $x = 0.0$  to 3.75 in. and is shown with momentum vectors indicating the bleed. The bleed momentum vectors are greater downstream of the shock impingement location because of higher pressures. The bleed boundary condition was used within the bleed region, while adiabatic, no-slip boundary conditions were used on the rest of the plate. The top boundary included the shock generator and was specified with an inviscid boundary condition. The right

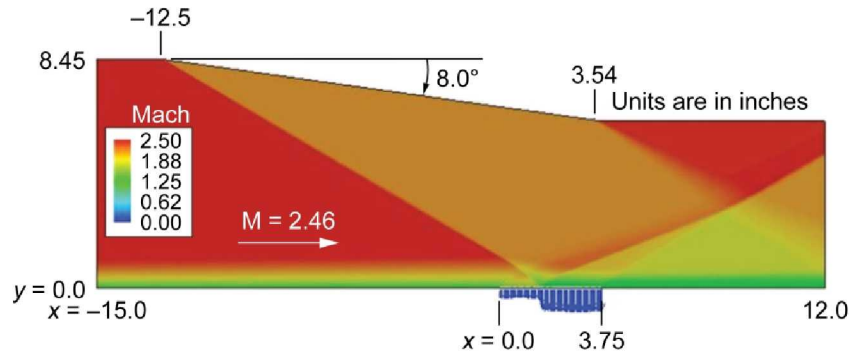


Figure 12.—Flow domain and Mach number contours for an oblique shock interacting with a bleed region on a flat plate.

boundary of the flow domain is a supersonic outflow boundary, and first-order extrapolation was used for the boundary condition.

The flow domain for the three-dimensional CFD simulations used an extrusion of the two-dimensional flow domain with the addition of eight bleed holes and the plenum. Figure 13 shows a view of the three-dimensional flow domain near the bleed holes. Geometric and flow symmetry was assumed to allow reflection boundaries at the midplanes of the holes. The flow domain for the two-dimensional simulations was extruded between adjacent hole centers to provide the depth in the  $z$ -direction between symmetry planes. The plenum was established arbitrarily to be large so as not to be an influence on the bleed rate. The shape of the plenum is similar to that shown in Figure 6 for the single-hole simulation. The bleed plenum is rectangular and extends from  $x = -8.13$  to  $10.0$  in. The bottom of the plenum is located at  $y = -16.25$  in. Attached to the bottom of the plenum is a converging nozzle block with its exit exhausting the plenum flow vertically downward. The exit is at  $y = -30.0$  in. A subsonic outflow boundary condition was applied at the plenum outflow, and the static pressure was specified. The bleed flow reaches very low speeds within the plenum, and the intent of the nozzle is to create a smooth exit for the bleed flow from the plenum. The walls of the plenum and bleed hole were specified as adiabatic, no-slip boundary conditions.

The grid for the two-dimensional flow domain consisted of a single, structured grid block with an H-grid. Wall spacing was set to achieve values  $y^+ = 4.0$  for the first grid point off the wall. A grid convergence study was performed to determine the grid spacing for which the bleed rate approached convergence. The results are shown in Table III. The Menter SST turbulence model was used for the simulations. The conclusion was that the streamwise spacing of  $0.4D$  was sufficient; however, the grid with streamwise spacing of  $0.2D$  was used to generate the sonic flow coefficients presented below. At the top surface of the domain, the wall spacing was set at  $0.02$  in. A hyperbolic tangent method was used to distribute grid points. In the vertical direction, 275 grid points were used and the maximum stretching between grid points was 3.4 percent, which occurred at the wall. In the streamwise direction, 369 grid points were distributed almost uniformly. The bleed region contained 75 grid points with grid spacing of  $0.05$  in., which was  $0.20D$ .

TABLE III.—GRID CONVERGENCE FOR AN OBLIQUE SHOCK INTERACTING WITH A BLEED REGION ON A FLAT PLATE

$\Delta s$ , in.	$\Delta s/D$	Hole grid size	$Q_{\text{sonic}}$	$ Q_{\text{sonic}} $ , percent
0.2	0.8	99 by 91	0.04657	3.93
0.1	0.4	185 by 161	0.04530	1.09
0.05	0.2	369 by 275	0.04478	0.07
0.025	0.1	739 by 501	0.04481	----

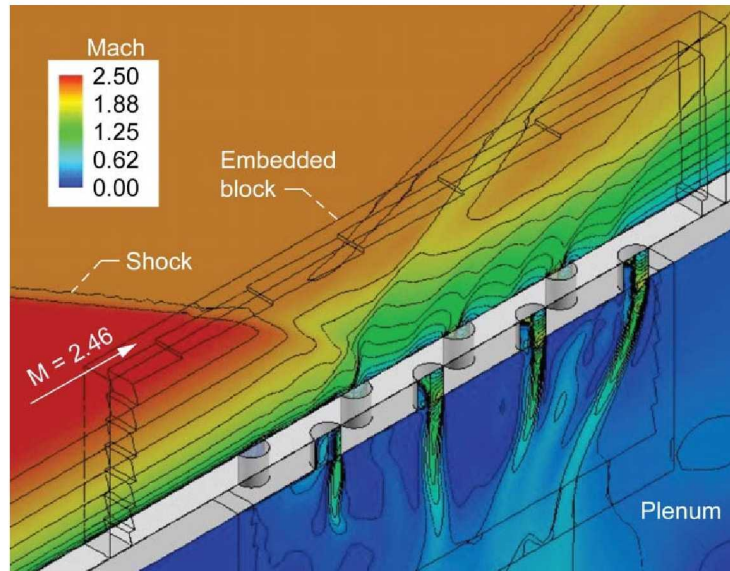


Figure 13.—Geometry and Mach number contours for an oblique shock interacting with a bleed region.

The grid for the three-dimensional simulations used the two-dimensional grid for the core flow of the tunnel containing the oblique shock. The two-dimensional grid was extruded in the  $z$ -direction of the three-dimensional domain. The information obtained for the single-hole simulation in the previous section was used to set the maximum grid spacing within the holes of  $0.04D$ . This required a grid block to be embedded on top of the bleed region and below the bleed region. The outline of the embedded blocks can be seen in Figure 13.

Figure 13 shows the Mach number contours in the vicinity of the bleed holes when the bleed flow rate is at its maximum. The flow is left to right with the oblique shock coming in from the left. The reflected shock and barrier shocks can be seen. The supersonic jets emanate from the bleed holes and extend into the plenum.

The variations of  $Q_{\text{sonic}}$  with respect to the plenum total pressure ratio for the experimental data and for the various CFD simulations are shown in Figure 14. The uncertainty of the experimental data was reported as 0.007 psi for static pressures, 0.045 psi for total pressures, and 2.4 percent for values of  $Q_{\text{sonic}}$ . The error bars for  $Q_{\text{sonic}}$  are shown in Figure 14, but those of the plenum total pressure ratio do not distinguish themselves from the plotting symbol. The plot labeled “Old BC” are the results presented in an earlier paper (Ref. 22) that used conditions at the edge of the boundary layer and performed a table lookup to obtain values of  $Q_{\text{sonic}}$ . As reported in the earlier paper, it was suggested that the old bleed boundary condition was not capable of indicating blowing from the bleed region. This resulted in erroneous values of plenum total pressure ratio between 0.12 and 0.16. Behind the shock impingement, the flow static pressure was high enough to cause bleeding. Ahead of the impingement, the local surface static pressure was less than the plenum static pressure, and the bleed holes should have exhibited blowing to set up recirculation within the bleed region. Such recirculation was observed in the wind tunnel experiment, even for plenum total pressure ratios as low as  $Q_{\text{sonic}} = 0.0342$ . The new bleed boundary condition uses the local surface static pressure and allows blowing through the use of the curve fit of Equation (13). Figure 14 shows the results of using the new bleed boundary condition for the two-dimensional CFD simulation. The recirculation was simulated and the comparison with the experimental data is improved as  $Q_{\text{sonic}}$  approached zero. Figure 15 illustrates the recirculation within the bleed region for the two-dimensional simulation with zero net bleed. A small separation region is shown with blowing ahead of the shock impingement and bleeding aft of the shock impingement.

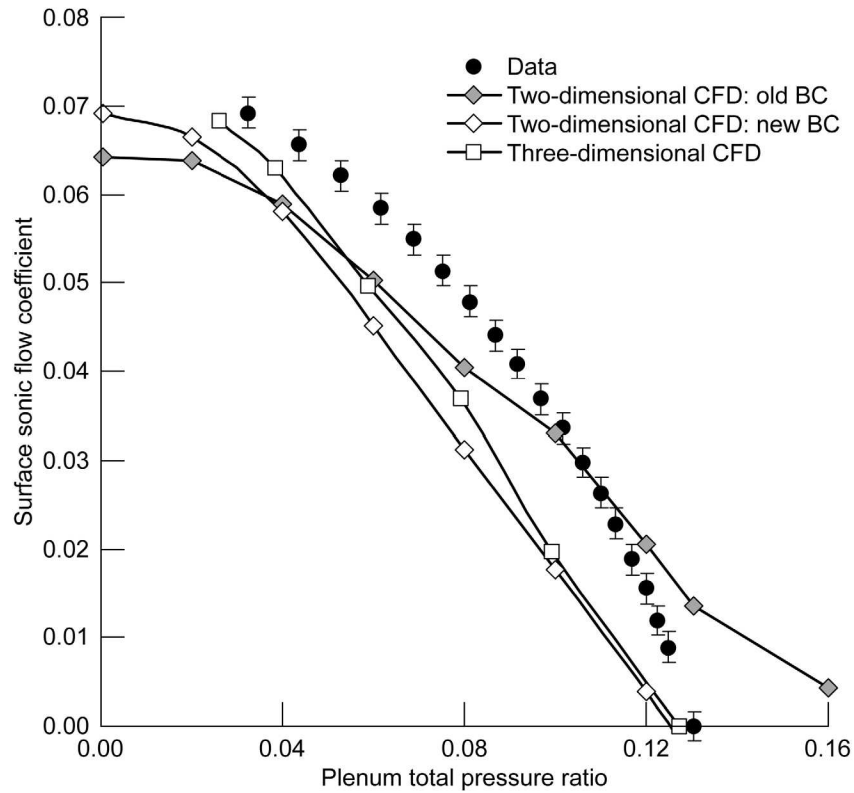


Figure 14.—Sonic flow coefficient distribution for a porous bleed region on a flat plate with an oblique-shock interaction.

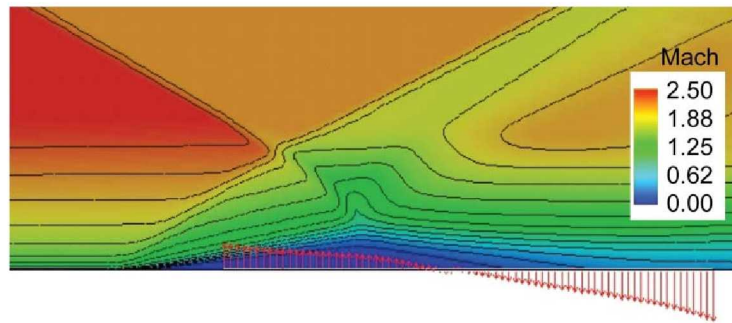


Figure 15.—Mach contours and bleed momentum vectors from a two-dimensional computational fluid dynamics simulation for an oblique shock interacting with bleed.

The  $Q_{\text{sonic}}$  variations for the three-dimensional simulations are also plotted in Figure 14. The results for the two-dimensional simulation using the new bleed boundary condition compare well with those of the three-dimensional simulation. This is encouraging and provides some verification of the improved bleed model. The fact that both the two-dimensional and three-dimensional CFD simulations indicate lower values of  $Q_{\text{sonic}}$  than the data suggest that perhaps factors such as turbulence modeling are the cause of the differences with the data.

Recirculation was also observed in the three-dimensional simulation at zero net bleed flow. Figure 16 shows the eight bleed holes with the momentum vectors drawn at the top of the holes along the symmetry planes. The first three holes show blowing, while the remaining five show bleeding.

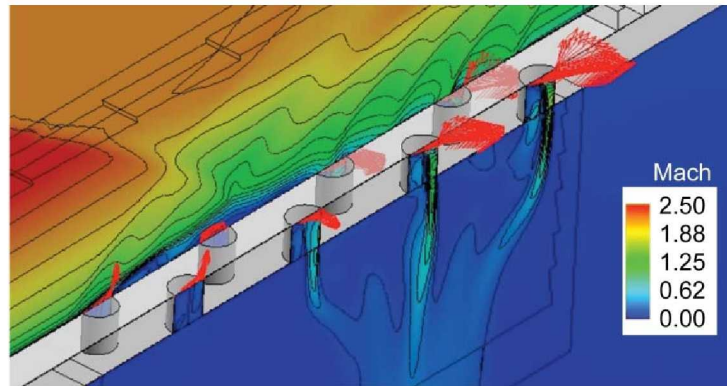


Figure 16.—Recirculation within the bleed region at zero net bleed.

## Conclusion

An improved bleed model was presented that used a scaling of the sonic flow coefficient data for 90° holes that allowed the local bleed flow to be computed based on the static pressure ratio across the bleed hole. A quadratic curve fit of the scaled data simplified the implementation of the bleed boundary condition into the Wind-US CFD code. Applying the bleed model in the simulation of bleed flows and three-dimensional simulations of the bleed holes with and without shocks resulted in several conclusions.

- The curve fit for the scaled sonic flow coefficient provided for a smooth variation of the sonic flow coefficient as the bleed flow approached net zero bleed.
- The curve fit provided for a rudimentary blowing condition that allowed simulation of recirculation within the bleed region.
- The three-dimensional CFD simulations of the flow within the bleed holes and plenum can provide sonic flow coefficient data for certain bleed configurations and flow conditions for which experimental data is not available. It may be possible to obtain the data with a single bleed hole, if hole interactions are not significant.
- The CFD simulations of a series of bleed holes interacting with an oblique shock demonstrated recirculation and good comparison to experimental data. These simulations are perhaps the first CFD simulations showing such interaction.

Further work is needed on developing bleed models for supersonic inlets. Future research needs to address the following questions:

- Can such scaling be applied to data for hole angles less than 90°?
- What effect do other bleed factors such as  $L/D$ ,  $D/\delta$ , or hole spacing have on the bleed flow, and how can such factors be modeled?
- What is the role of the tangential velocity component in modeling bleed flows? Is this related to the bleed roughness effect? How should such features be modeled?

## References

1. Seddon, J.: Intake Aerodynamics. AIAA Education Series, New York, NY, 1985.
2. Syberg, J.; and Hickcox, T.E.: Design of a Bleed System for a Mach 3.5 Inlet. NASA CR-2187, 1973.
3. Tjonneland, E.: The Design, Development, and Testing of a Supersonic Transport Intake System. AGARD-CP-91-71, 1971.

4. Delery, J.M.: Shock Wave/Turbulent Boundary Layer Interaction and Its Control. *Prog. Aerosp. Sci.*, vol. 22, no. 4, 1985, pp. 209–280.
5. Hamed, A.; and Shang, J.S.: Survey of Validation Data Base for Shockwave Boundary-Layer Interactions in Supersonic Inlets. *J. Propulsion*, vol. 7, no. 4, 1991, pp. 617–625.
6. Fukuda, M.K.; Hingst, W.R.; and Reshotko, E.: Bleed Effects on Shock/Boundary-Layer Interactions in Supersonic Mixed Compression Inlets. *J. Aircraft*, vol. 14, no. 2, 1977, pp. 151–156.
7. Cubbison, R.W.; and Sanders, B.W.: Effect of Bleed-System Back Pressure and Porous Area on the Performance of an Axisymmetric Mixed-Compression Inlet at Mach 2.50. NASA TM X-1710, 1968.
8. Shaw, R.J.; Wasserbauer, J.F.; and Neumann, H.E.: Boundary Layer Bleed System Study for a Full-Scale, Mixed-Compression Inlet With 45 Percent Internal Contraction. NASA TM X-3358, 1976.
9. Mitchell, G.A.; and Sanders, B.W.: Increasing the Stable Operating Range of a Mach 2.5 Inlet. NASA TM X-52799, 1970.
10. Paynter, Gerald C.; Mayer, David W.; and Tjonneland, Elling: Flow Stability Issues in Supersonic Inlet Flow Analyses. AIAA-1993-290, 1993.
11. Mayer, David W.: Prediction of Supersonic Inlet Unstart Caused by Freestream Disturbances. *AIAA J.*, vol. 33, no. 2, 1995, pp. 266–275.
12. Hedges, Linda S., et al.: Supersonic Inlet Simulation With Closed-Loop Control of Moving Control Surfaces. AIAA-1996-493, 1996.
13. Slater, John W., et al.: Role of CFD in the Aerodynamic Design and Analysis of the Parametric Inlet. ISABE-2005-1168, 2005.
14. Abrahamson, K.W.; and Brower, D.L.: An Empirical Boundary Condition for Numerical Simulation of Porous Plate Bleed Flows. AIAA-88-0306, 1988.
15. Chyu, W.J.; Howe, G.W.; and Shih, T.I-P.: Bleed-Boundary Conditions for Numerically Simulated Mixed-Compression Supersonic Inlet Flow. *J. Propul. P.*, vol. 8, no. 4, 1992, pp. 862–868.
16. Paynter, Gerald C.; Treiber, David A.; and Kneeling, W.D.: Modeling Supersonic Inlet Boundary-Layer Bleed Roughness. *J. Propul. P.*, vol. 9, no. 4, 1993, pp. 622–627.
17. Mayer, David W.; and Paynter, Gerald C.: Boundary Conditions for Unsteady Supersonic Inlet Analyses. *AIAA J.*, vol. 32, no. 6, 1994, pp. 1200–1206.
18. Harloff, Gary J.; and Smith, Gregory E.: Supersonic-Inlet Boundary-Layer Bleed Flow. *AIAA J.*, vol. 34, no. 4, 1996, pp. 778–785.
19. Dambara, Shinsuke; Yamamoto, Makoto; and Honami, Shinji: Modeling of Boundary Condition for Turbulent Boundary Layer Bleed. AIAA-98-0926, 1998.
20. Benson, D.B., et al.: Boundary Conditions for CFD Simulations of Supersonic Boundary-Layer Bleed Through Discrete Holes. AIAA-2000-0888, 2000.
21. Akatsuka, J., et al.: Porous Bleed Model for Boundary Condition of CFD Analysis. AIAA 2006-3682, 2006.
22. Slater, John W.; and Saunders, John D.: Modeling of Fixed-Exit Porous Bleed Systems. AIAA 2008-94, 2008.
23. Mani, M.; Cary, A.; and Ramakrishnan, S.V.: A Structured and Hybrid-Unstructured Grid Euler and Navier-Stokes Solver for General Geometry. AIAA-2004-524, 2004.
24. McLafferty, G.; and Ranard, E.: Pressure Losses and Flow Coefficients of Slanted Perforations Discharging From Within a Simulated Supersonic Inlet. R-0920-1, United Aircraft Corp., East Hartford, CT, 1958.
25. Willis, B.P.; Davis, D.O.; and Hingst, W.R.: Flow Coefficient Behavior for Boundary Layer Bleed Holes and Slots. AIAA-95-0031, 1995.
26. Willis, B.P.; and Davis, D.O.: Boundary Layer Development Downstream of a Bleed Mass Flow Removal. AIAA-96-3278, 1996.
27. Hamed, A.; Yeuan, J.J.; and Jun, Y.D.: Flow Characteristics in Boundary-Layer Bleed Slots With Plenum, *J. Propul. P.*, vol. 12, no. 2, 1996, pp. 231–236.

28. Davis, D.O.: Fundamental Bleed Experiments at NASA Glenn Research Center 1995–1999. Presentation at a Shock Wave/Boundary Layer Interaction Workshop at NASA Glenn Research Center, April 2008, unpublished.
29. White, Frank M.: Viscous Fluid Flow. McGraw-Hill, New York, NY, 1974.
30. Hamed, Awatef; and Li, Zhisong: Simulation of Bleed-Hole Rows for Supersonic Turbulent Boundary Layer Control. AIAA 2008–67, 2008.
31. Bodner, J.P., et al.: Experimental Investigation of the Effect of a Single Bleed Hole on a Supersonic Turbulent Boundary-Layer. AIAA–96–2797, 1996.
32. Bodner, Jeffrey Paul: Experimental Investigation of the Effect of a Single Bleed Hole on a Turbulent Supersonic Boundary-Layer. M.S. Thesis, Case Western Reserve Univ., 1996.
33. Shih, T.I-P.; Rimlinger, M.J.; and Chyu, W.J.: Three-Dimensional Shock-Wave/Boundary-Layer Interactions With Bleed. AIAA J., vol. 31, no. 10, 1993, p. 1819.
34. Willis, B.P.; Davis, D.O.; and Hingst, W.R.: Flowfield Measurements in a Normal-Hole-Bled Oblique Shock-Wave and Turbulent Boundary-Layer Interaction. AIAA–95–2885, 1995.
35. Harloff, G.J.; and Smith, G.E.: Numerical Simulation of Supersonic Flow Using a New Analytical Bleed Boundary Condition. AIAA 95–2759, 1995.
36. Rimlinger, Mark J., et al.: Computations of Shock-Wave/Boundary-Layer Interactions With Bleed. AIAA–96–0432, 1996.

REPORT DOCUMENTATION PAGE			Form Approved OMB No. 0704-0188		
<p>The public reporting burden for this collection of information is estimated to average 1 hour per response, including the time for reviewing instructions, searching existing data sources, gathering and maintaining the data needed, and completing and reviewing the collection of information. Send comments regarding this burden estimate or any other aspect of this collection of information, including suggestions for reducing this burden, to Department of Defense, Washington Headquarters Services, Directorate for Information Operations and Reports (0704-0188), 1215 Jefferson Davis Highway, Suite 1204, Arlington, VA 22202-4302. Respondents should be aware that notwithstanding any other provision of law, no person shall be subject to any penalty for failing to comply with a collection of information if it does not display a currently valid OMB control number.</p> <p>PLEASE DO NOT RETURN YOUR FORM TO THE ABOVE ADDRESS.</p>					
<b>1. REPORT DATE (DD-MM-YYYY)</b> 01-06-2009		<b>2. REPORT TYPE</b> Technical Memorandum		<b>3. DATES COVERED (From - To)</b>	
<b>4. TITLE AND SUBTITLE</b> Improvements in Modeling 90° Bleed Holes for Supersonic Inlets			<b>5a. CONTRACT NUMBER</b>		
			<b>5b. GRANT NUMBER</b>		
			<b>5c. PROGRAM ELEMENT NUMBER</b>		
<b>6. AUTHOR(S)</b> Slater, John, W.			<b>5d. PROJECT NUMBER</b>		
			<b>5e. TASK NUMBER</b>		
			<b>5f. WORK UNIT NUMBER</b> WBS 984754.02.07.03.13.02		
<b>7. PERFORMING ORGANIZATION NAME(S) AND ADDRESS(ES)</b> National Aeronautics and Space Administration John H. Glenn Research Center at Lewis Field Cleveland, Ohio 44135-3191			<b>8. PERFORMING ORGANIZATION REPORT NUMBER</b> E-16888		
<b>9. SPONSORING/MONITORING AGENCY NAME(S) AND ADDRESS(ES)</b> National Aeronautics and Space Administration Washington, DC 20546-0001			<b>10. SPONSORING/MONITOR'S ACRONYM(S)</b> NASA		
			<b>11. SPONSORING/MONITORING REPORT NUMBER</b> NASA/TM-2009-215597; AIAA-2009-0710		
<b>12. DISTRIBUTION/AVAILABILITY STATEMENT</b> Unclassified-Unlimited Subject Categories: 02 and 07 Available electronically at <a href="http://gltrs.grc.nasa.gov">http://gltrs.grc.nasa.gov</a> This publication is available from the NASA Center for AeroSpace Information, 443-757-5802					
<b>13. SUPPLEMENTARY NOTES</b>					
<b>14. ABSTRACT</b> The modeling of porous bleed regions as boundary conditions in computational fluid dynamics (CFD) simulations of supersonic inlet flows has been improved through a scaling of sonic flow coefficient data for 90° bleed holes. The scaling removed the Mach number as a factor in computing the sonic flow coefficient and allowed the data to be fitted with a quadratic equation, with the only factor being the ratio of the plenum static pressure to the surface static pressure. The implementation of the bleed model into the Wind-US CFD flow solver was simplified by no longer requiring the evaluation of the flow properties at the boundary-layer edge. The quadratic equation can be extrapolated to allow the modeling of small amounts of blowing, which can exist when recirculation of the bleed flow occurs within the bleed region. The improved accuracy of the bleed model was demonstrated through CFD simulations of bleed regions on a flat plate in supersonic flow with and without an impinging oblique shock. The bleed model demonstrated good agreement with experimental data and three-dimensional CFD simulations of bleed holes.					
<b>15. SUBJECT TERMS</b> Supersonic inlets; Inlet flow					
<b>16. SECURITY CLASSIFICATION OF:</b>			<b>17. LIMITATION OF ABSTRACT</b>	<b>18. NUMBER OF PAGES</b> 27	<b>19a. NAME OF RESPONSIBLE PERSON</b> STI Help Desk (email: <a href="mailto:help@sti.nasa.gov">help@sti.nasa.gov</a> )
<b>a. REPORT</b> U	<b>b. ABSTRACT</b> U	<b>c. THIS PAGE</b> U			<b>19b. TELEPHONE NUMBER (include area code)</b> 443-757-5802



